




Design of lead-free PVDF/CNT/BaTiO₃ piezocomposites for sensing and energy harvesting: the role of polycrystallinity, nanoadditives, and anisotropy

Jagdish A Krishnaswamy^{1,5} , Federico C Buroni²,
Enrique García-Macías³ , Roderick Melnik^{1,4},
Luis Rodriguez-Tembleque⁴  and Andres Saez⁴

¹ MS2Discovery Interdisciplinary Research Institute, Wilfrid Laurier University, 75 University Ave W, Waterloo, N2L 3C5, Ontario, Canada

² Department of Mechanicals Engineering and Manufacturing, Universidad de Sevilla, Camino de los Descubrimientos s/n, Seville E-41092, Spain

³ Department of Civil and Environmental Engineering, University of Perugia, Via G Duranti 93, Perugia I-06125, Italy

⁴ Department of Continuum Mechanics and Structural Analysis, Universidad de Sevilla, Camino de los Descubrimientos s/n, Seville E-41092, Spain

E-mail: ajagdish@wlu.ca

Received 7 August 2019, revised 9 October 2019

Accepted for publication 5 November 2019

Published 2 December 2019



Abstract

Lead-free piezoelectric composites with polymeric matrices offer a scalable and eco-friendly solution to sensing and energy harvesting applications. Piezoelectric polymers such as PVDF are particularly interesting because of the possibility to engineer the performance of these materials through addition of higher-performance piezoelectric inclusions and nanomaterials and to scalably manufacture such composites by emerging techniques such as 3D printing. This work makes two contributions, namely towards composite design and towards development of accurate effective property models. In the context of composite design, we evaluate the piezoelectric performance of PVDF modified by the addition of polycrystalline-BaTiO₃ and multiwalled carbon nanotubes. Firstly, the addition of BaTiO₃ dramatically improves the electric field within the composite offering significant advantages specially at low BaTiO₃ concentrations. Secondly, the addition of carbon nanotubes to the matrix, particularly at higher BaTiO₃ loadings, leads to an order of magnitude increase in the piezoelectric flux generation. Further enhancement in the flux generation is also possible by tuning the polycrystallinity of the BaTiO₃ inclusions. However, these behaviours are inclusion-driven and the piezoelectric behaviour of the matrix does not contribute to this improvement. Importantly, a small addition of BaTiO₃ and CNT into the PVDF matrix, away from percolation, can simultaneously improve flux and electric field generation. In this part of the work, we assume an isotropic PVDF matrix. Given that PVDF is elastically anisotropic, the second aspect of this work is the development of an effective property model for CNT-modified PVDF, taking into account the elastic anisotropy of poled PVDF, to predict the elastic coefficients of CNT-modified PVDF matrices, thus undertaking a key step towards modelling anisotropic piezoelectric composites. We show that the anisotropy-based model makes similar predictions in the effective composite behaviour, indicating that in the case of

⁵ Author to whom any correspondence should be addressed

PVDF-based piezocomposites, the anisotropy of the matrix does not significantly affect the piezoresponse.

Keywords: lead-free piezoelectric, composite, polycrystal, carbon nanotube, multiscale design and homogenization, finite element analysis, smart materials

(Some figures may appear in colour only in the online journal)

1. Introduction

Piezoelectric composites based on lead-free materials are scalable and environmentally friendly solutions to applications in sensing and harvesting of mechanical energy and in electro-mechanical actuation [1–3]. Such composites typically consist of nano- or microparticles of rigid crystalline lead-free piezoelectric materials such as BaTiO₃, which exhibit high piezoelectric activity, in relatively softer matrices, typically polymers [4–7]. Optimum combination of these two material components can lead to applications in infrastructure, wearable electronics, robotics and so on [2, 6, 8, 9]. The intrinsic piezoelectricity of certain matrices such as PVDF, PVDF-TrFE etc, offer an additional degree of freedom in the design of such composite materials. PVDF is a piezoelectric polymer which has demonstrated to be a promising candidate for applications in flexible electronics, among many others [4, 7, 9], owing to the possibility of scalable fabrication of its composites by emerging technologies such as 3D printing [4, 7]. 3D printing further offers prospects to tune the micro and macrostructures of the composite materials thus allowing a fine control over the anisotropic response of the final composite structure [5, 10]. However, the polymer exhibits a weak piezoelectric response [11], which can be further tuned by the addition of high-performance piezoelectric inclusions and nanomaterials such as carbon nanotubes [12–15]. The addition of carbon nanotubes has been shown to improve both the piezoelectric flux generation and the electric field generation within the piezoelectric composite [14], which are both important for efficient devices [2]. While experiments have demonstrated the advantages of such composite design in enhancing the performance of PVDF-based piezoelectric composite materials, there are several details that remain unclear and warrant further investigation. These include uncovering the role of the nanomaterial addition, the polycrystalline nature of the piezoelectric inclusions and understanding the significance of the intrinsic piezoelectricity of the matrix. Experimental investigations, till date, have considered a small subset of the material design space for improved performances. However, a computational approach, as undertaken in this work, can lead to important insights on the details of the roles of each component of the composite and the contexts under which they are effective. The results of such an approach can give directions to the design of superior composites for specific applications such as energy harvesting and sensing. This will enable an optimal choice of materials for the composite, depending on the application. Here, we consider a lead-free piezocomposite comprising of a PVDF polymeric matrix with polycrystalline BaTiO₃ piezoelectric inclusions. The matrix is further modified with multiwalled carbon

nanotubes. Through better mechanical and electrical networks provided by the carbon-nanotube fillers, this design strategy has been demonstrated to lead to superior performances in the aspect of strain-sensing [12]. In the first part of our discussions, we will evaluate the roles of the polycrystalline nature of the BaTiO₃ inclusions, the percolative effect of the carbon nanotube fillers, and the piezoelectricity of the PVDF matrix in tuning composite behaviour for specific applications. We obtain these initial results assuming an elastically isotropic PVDF matrix. Given that PVDF is an elastically anisotropic polymer [11], it is necessary to develop better effective property models for CNT-modified PVDF which take into account the elastic anisotropy of the matrix. In the second part of this work, we develop a new model to predict the effective elastic coefficients of the CNT-modified PVDF while simultaneously accounting for the anisotropy in the mechanical properties. Further, the results of these two approaches are compared to evaluate the role of the elastic anisotropy in the final piezoelectric response of the composite. Therefore, while this work firstly provides important insights to the design of nanomodified PVDF-based lead-free composite materials for sensing and energy harvesting, it also takes an important step towards developing accurate material models for anisotropic-matrix-based composite materials.

2. Model

In this section, we provide details of the coupled electro-elastic model describing the piezoelectric response of the composites. Firstly, section 2.1 provides details of the governing and phenomenological relations and the material models that are adopted for the matrix and the inclusions. Here, it is assumed that PVDF is mechanically isotropic. In section 2.2, we present the details of the model which predicts the effective elastic coefficients of the CNT-modified PVDF, starting from the anisotropic elastic behaviour of PVDF.

2.1. Electro-elastic model and basic material models

The composite architecture is a two-dimensional RVE consisting of randomly shaped and randomly positioned BaTiO₃ inclusions in a square matrix, in the x_1 – x_3 plane. The matrix has sides $a_m = b_m = 50 \mu\text{m}$ (figure 1(a)). It further contains multiwalled carbon nanotubes (MWCNTs). The electro-elastic behaviour of these matrices are modelled by the phenomenological relations (equation (1)) and the governing equations (equation (2)), given by (e.g. [16, 17]):

$$\sigma_{ij} = c_{ijkl}\varepsilon_{kl} - e_{kij}E_k, \quad D_i = \epsilon_{ij}E_j + e_{ijk}\varepsilon_{jk}, \quad (1)$$

$$\sigma_{ij,j} = 0, \quad D_{i,i} = 0, \quad (2)$$

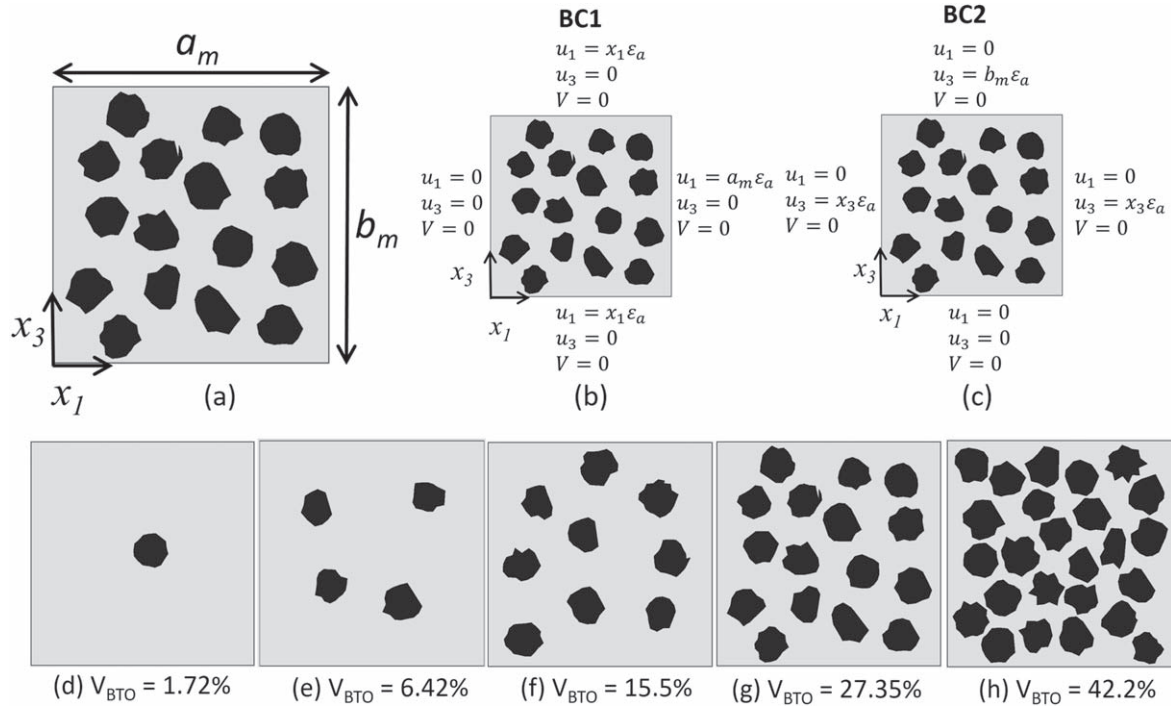


Figure 1. (a) A representative schematic of the RVE that is investigated here, with the axis system, (b) and (c) schematically show the boundary conditions BC1 and BC2 that are used in the analysis, (d)–(h) show the 5 RVE architectures used for our simulations. The volume fractions V_{BTO} of the BaTiO_3 microscale inclusions are specified. The matrix is either PVDF (piezoelectric) or epoxy (non-piezoelectric).

where σ_{ij} and ε_{ij} are the components of stress and strain tensors, respectively, and E_i and D_i are the components of the electric field and the electric flux density vectors, respectively. Further, c_{ijkl} , e_{ijk} , ϵ_{ij} are the elastic, piezoelectric and the permittivity coefficients of the constituent materials of the composite. The strain tensor is related to the displacement vector as $\varepsilon_{ij} = \frac{1}{2}(u_{i,j} + u_{j,i})$. The details of the two-dimensional implementation of this model and the algorithms to generate randomly shaped inclusions can be found elsewhere [16]. The model outlined here is implemented and solved using finite element analysis with a maximum element size of 1 micrometer. Particular solutions to the above equations are obtained by subjecting the RVE to two different boundary conditions shown in figures 1(b), (c). Boundary conditions BC1 and BC2 are used to obtain the effective piezoelectric coefficients e_{31} and e_{33} , respectively [16, 17]. These two boundary conditions are chosen because for the two-dimensional architecture considered here, e_{31} and e_{33} are the transverse and longitudinal piezoelectric coefficients of interest. Figures 1(d)–(h) further show the 5 RVEs with different BaTiO_3 volume fractions, V_{BTO} , investigated in the current analysis. The microscale inclusions are randomly shaped and randomly positioned. The randomly shaped inclusions are bounded within two concentric circles with radii R_1 and R_2 , which are randomly selected in the ranges $[2.5 \mu\text{m}, 3.5 \mu\text{m}]$ and $[4 \mu\text{m}, 5 \mu\text{m}]$, respectively. The inclusions are modelled as polygons having n sides, where n is chosen randomly in the range [10, 18]. The detailed algorithm for the generation of the random geometry is given in [16]. The size of the inclusions, i.e. a few micrometers, has been chosen such that the inclusions are larger than the optimum

BaTiO_3 grain sizes required for the best known piezoelectric response, which is just smaller than a micron [19]. While larger piezoelectric inclusions could be used, it is important to retain optimal grain sizes. Smaller inclusions can also be used. However, it is possible that very small inclusions might just contain a single grain with all the dipoles oriented similarly, resembling a single crystal. We will see in the results that under certain conditions, polycrystalline inclusions show a better performance. Therefore, the inclusion size of a few microns which, can exhibit polycrystalline properties, has been chosen. As pointed out earlier, these polycrystalline properties can also be exhibited by even larger inclusions.

We next briefly discuss the material properties used in this investigation. (15, 15) Multiwalled carbon nanotubes (MWCNTs), with an aspect ratio around 100 are assumed to be uniformly dispersed in the matrix without agglomerations. Addition of carbon nanotubes affects the dielectric and piezoelectric properties of the PVDF matrix [20, 18, 21, 22]. Based on experimental observations [21–23], the dielectric behaviour of the matrix can be described by a percolative behaviour given by:

$$\epsilon_m^{\text{eff}} = \epsilon_m \left(\frac{f_c}{f_c - f_{\text{CNT}}} \right)^p, \quad (3)$$

where ϵ_m and ϵ_m^{eff} are the permittivity of the pristine and the modified matrices respectively, f_c and p are the percolation threshold and critical exponent for MWCNTs in the PVDF matrix, and f_{CNT} is the volume fraction of the MWCNTs in the matrix. As the concentration of the nanotubes increases, there is a rapid increase in the permittivity specifically as f_{CNT} approaches f_c . Under the assumptions of non-agglomerated

Table 1. Electro-elastic material constants used in the simulations ((λ_{m1} , μ_{m1}) and (λ_{m2} , μ_{m2}) refer to the Lamé's constants of the elastically isotropic PVDF and epoxy matrices, respectively).

Material property	Values for BaTiO ₃	Values for PVDF	Values for epoxy
Elastic properties (Moduli in Pa)			
c_{11}	275.1×10^9 [24]	$\lambda_{m1} + 2\mu_{m1}$	$\lambda_{m2} + 2\mu_{m2}$
c_{13}	151.55×10^9	λ_{m1}	λ_{m2}
c_{33}	164.8×10^9	$\lambda_{m1} + 2\mu_{m1}$	$\lambda_{m2} + 2\mu_{m2}$
c_{44}	54.3×10^9	μ_{m1}	μ_{m2}
Young's modulus, E_m	N.A.	2.0×10^9 [28]	3.5×10^9 (from datasheet)
Poisson's ratio, ν_m	N.A.	0.29	0.35
Relative permittivity			
ϵ_{11}/ϵ_0	1970 [24]	8 [29]	3.5 [30]
ϵ_{33}/ϵ_0	109	8	3.5
Piezoelectric coefficients (Cm ⁻²)			
e_{15}	21.3 [24]	0 [11]	Matrix is non-piezoelectric ($e_{ij} = 0$)
e_{31}	-2.69	0.024	
e_{33}	3.65	-0.027	

CNTs having an aspect ratio of roughly 100, which are uniformly dispersed in the PVDF matrix, we have $f_c = 1.14\%$ and $p = 1.0068$ [21]. We use these values of the percolation parameters for our study.

Although the piezoelectric coefficients which are intricately related to the β -phase of PVDF, are modified by the addition of carbon nanotubes, they are not very sensitive to the nano-addition [18, 20], and hence we assume their constant values equal to that of the pristine PVDF matrices. The polycrystallinity of the BaTiO₃ inclusions affects the effective electro-elastic properties [19, 24], the model and implementation of which have been discussed earlier [16]. The effective properties are obtained starting from the electro-elastic coefficients of single-crystal BaTiO₃ [24]. The polycrystalline properties are defined using an orientation parameter α , with $\alpha \rightarrow 0$ and $\alpha \rightarrow \infty$, respectively corresponding to the single crystalline and randomly oriented extremes. Intermediate values of α represent controlled randomness with preferential orientation along the c -axis of BaTiO₃ (here, it is the x_3 axis or the poling direction). A summary of the material properties used for this investigation is given in table 1. In addition to PVDF, we carry out simulations on a non-piezoelectric matrix (epoxy- araldite LY5052), which has elastic properties similar to that of PVDF. This comparison will facilitate the understanding of the role of the piezoelectricity of the matrix in determining the piezoelectric performance of the composite and its usefulness in specific applications. For the elastic properties of the PVDF matrix, isotropic behaviour is assumed for a simplified calculation of its effective elastic properties on addition of CNTs, based on the approaches outlined in [25–27].

In short, a two-parameter model is used to describe the volume fraction and the state of agglomeration of CNTs in the matrix, and in this particular case, we assume a matrix with uniformly distributed CNTs without agglomerations. Since the PVDF matrix is assumed to be isotropic, the elastic properties of interest are the isotropic Young's modulus E_m and the Poisson's ratio ν_m . These are determined by using a two-parameter model described in [25–27]. The plots of E_m and ν_m , as functions of the CNT volume fraction f_{CNT} , are shown in figures 2(a) and (b). To obtain the elastic coefficients c_{ij} , first the Lamé's constants, given by $\lambda_m = \frac{E_m \nu_m}{(1 + \nu_m)(1 - 2\nu_m)}$ and $\mu_m = \frac{E_m}{2(1 + \nu_m)}$, are calculated. Then, the effective elastic coefficients are calculated as $c_{11} = c_{33} = \lambda_m + 2\mu_m$, $c_{13} = \lambda_m$, and $c_{44} = \mu_m$. The effective elastic coefficients, as functions of f_{CNT} , are shown in figure 2(c). It is seen that all the effective coefficients show a near linear dependence on f_{CNT} which is also observed in experiments [20].

2.2. The effective properties of CNT-modified PVDF starting from anisotropic elastic properties

In the previous section, we considered the effective elastic properties of PVDF modified by CNTs, while assuming isotropic elastic coefficients. However, PVDF is an anisotropic polymer [11]. To accurately predict the piezoelectric response of composites of such materials, it is important to develop materials models which account for the material anisotropy. Here we develop the effective elastic coefficients of the CNT-modified PVDF matrix starting from the anisotropic mechanical properties of the PVDF matrix coupled with the transversely isotropic mechanical properties of CNTs.

A classical Mori–Tanaka model is used in order to estimate the mechanical properties of the PVDF matrix doped with randomly oriented straight CNTs, with a volume fraction f_{CNT} . Consider a CNT as a nano-inclusion with ellipsoidal shape given by $\left(\frac{x'_1}{a_1}\right)^2 + \left(\frac{x'_2}{a_2}\right)^2 + \left(\frac{x'_3}{a_3}\right)^2 = 1$, where a_1 , a_2 , and a_3 are the lengths of the semi-axes of the ellipsoid fixed to a Cartesian coordinate system x'_i ($i = 1, 2, 3$) (see figure 2(d)). In this framework the effective elastic moduli can be expressed as follows:

$$\mathbf{C} = \mathbf{C}_m + f_{CNT} [\mathbf{C}_{CNT} \mathbf{A} - \mathbf{C}_m \mathbf{A}], \quad (4)$$

where \mathbf{C}_m and \mathbf{C}_{CNT} are respectively the orthotropic elasticity tensor of the PVDF matrix and the elasticity tensor of the transversely isotropic equivalent inclusion for the (15, 15) MWCNT, where the isotropy axis is coincident with the major semi-axis x'_3 (see figure 2(d)). Table 2 summarizes the corresponding non-vanishing Voigt coefficients for \mathbf{C}_m and \mathbf{C}_{CNT} referred to x_i ($i = 1, 2, 3$) and x'_i ($i = 1, 2, 3$), respectively. Note that equation (4) is referred to the fixed Cartesian coordinate system x_i ($i = 1, 2, 3$). In equation (4), \mathbf{A} is the strain concentration tensor that relates the average strain in the CNT to that compatible with applied uniform displacement boundary conditions on the surface of the system PVDF + CNT. The concentration tensor is given by

$$\mathbf{A} = \mathbf{A}^{dil} [(1 - f_{CNT}) \mathbf{I} + f_{CNT} \mathbf{A}^{dil}]^{-1}, \quad (5)$$

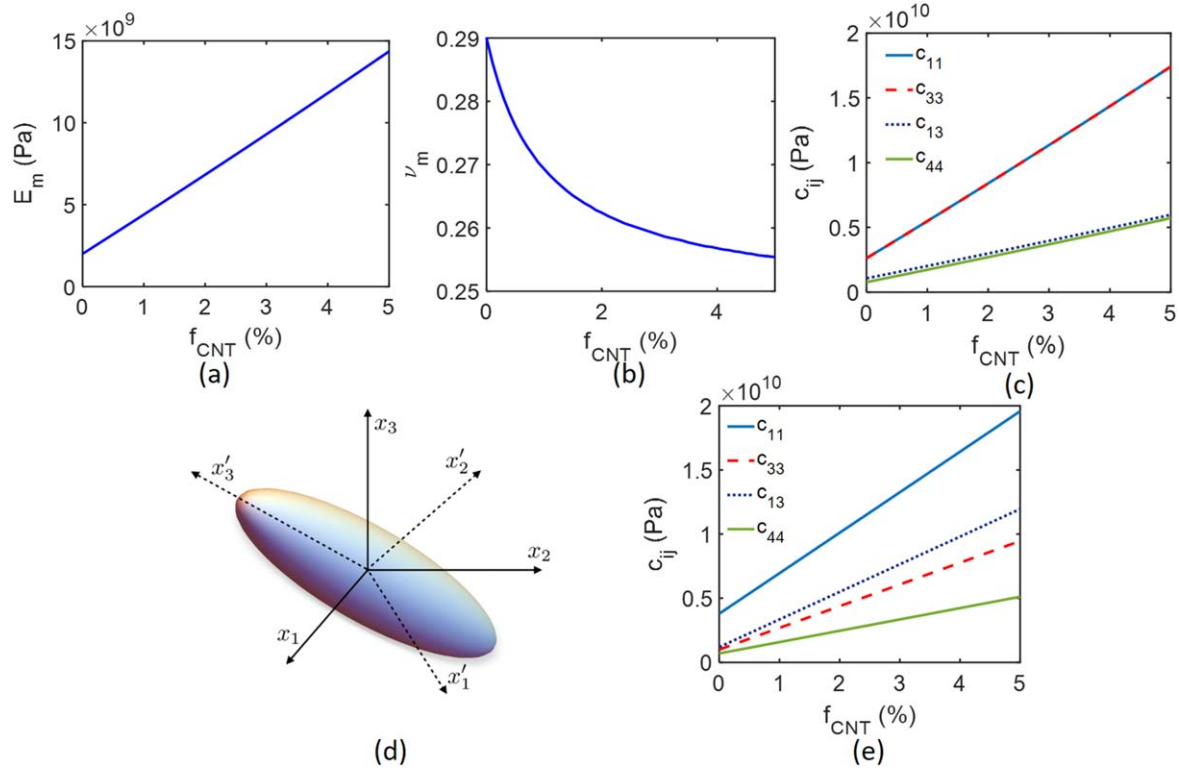


Figure 2. The effective elastic properties of the CNT-modified isotropic PVDF matrix viz. (a) the effective Young's modulus, (b) the effective Poisson's ratio, and (c) the effective elastic coefficients. (d) the ellipsoidal CNT nanoinclusion with the associated coordinate systems—the x_i ($i = 1, 2, 3$) global Cartesian coordinate system fixed to the matrix and the x'_i ($i = 1, 2, 3$) local Cartesian coordinate system fixed to the nanoinclusion. (e) The effective elastic properties of CNT-modified PVDF derived from the anisotropic elastic properties of PVDF.

Table 2. Anisotropic Elastic coefficients of PVDF and (15, 15) MWCNTs.

Coefficient (in GPa)	PVDF [11]	(15, 15) MWCNT [26]
c_{11}	3.8	230.1
c_{12}	1.9	211.9
c_{13}	1.0	66.3
c_{22}	3.2	230.1
c_{23}	0.9	66.3
c_{33}	1.2	1429.9
c_{44}	0.7	398
c_{55}	0.9	398
c_{66}	0.9	9.1

where \mathbf{I} is the fourth-order symmetric identity tensor

$$(\mathbf{I})_{ijkl} = \frac{1}{2}(\delta_{ik}\delta_{jl} + \delta_{il}\delta_{jk}) \quad (6)$$

δ_{ij} being the Kronecker delta and \mathbf{A}^{dil} the dilute concentration tensor given by

$$\mathbf{A}^{\text{dil}} = [\mathbf{I} + \mathbf{S}\mathbf{C}_m^{-1}(\mathbf{C}_{\text{CNT}} - \mathbf{C}_m)]^{-1}. \quad (7)$$

Here the fourth-order Eshelby tensor \mathbf{S} is a function of the orthotropic elasticity \mathbf{C}_m , and the ellipsoidal shape of the nanoinclusion $\left(\frac{a_2}{a_1} = \frac{a_2}{a_3} = \frac{L_{\text{CNT}}}{2R_{\text{CNT}}}\right)$. Its components in the x'_i ($i = 1, 2, 3$) coordinate system, S'_{mnab} , can be obtained by carrying out by integration over unit sphere in \mathbb{R}^3 , which after

transformation reads [31]

$$S'_{mnab} = \frac{1}{8\pi}(\mathbf{C}'_m)_{ijab} \int_{-1}^1 \int_0^{2\pi} [J'_{mjn}(\mathbf{z}) + J'_{njm}(\mathbf{z})] d\beta d\xi_3. \quad (8)$$

Above, $J'_{mjn}(\mathbf{z}) = K_{mj}^{-1}(\mathbf{z})z_i z_n$, where K_{mj}^{-1} is the inverse of the Christoffel tensor $K_{kj}(\mathbf{z}) = K_{jk}(\mathbf{z}) = (\mathbf{C}'_m)_{ijkm}z_i z_m$ and \mathbf{z} is a unit vector whose components are expressed as functions of integration variables by $z_1 = \frac{\sqrt{1-\xi_3^2} \cos \beta}{a_1}$, $z_2 = \frac{\sqrt{1-\xi_3^2} \sin \beta}{a_2}$, and $z_3 = \xi_3$. In this work, the evaluation of the Eshelby tensor is performed by numerical integration where we adopt a local adaptive strategy which recursively parts the subregion into smaller disjoint subregions and computes integral and error estimates for each of them. From equation (8), the Eshelby tensor can be obtained in the x_i ($i = 1, 2, 3$) coordinate system through proper tensorial transformation. Angled brackets in equation (4) denote the orientational average of a tensor function of $(\psi, \xi = \cos \theta, \phi)$

$$\langle \cdot \rangle = \int_0^{2\pi} \int_0^{2\pi} \int_{-1}^{+1} (\cdot) d\xi d\psi d\phi, \quad (9)$$

where (θ, ψ, ϕ) are the Euler angles. In this work, we adopt the following order for the rotations: one begins with the coordinate system x'_i ($i = 1, 2, 3$) fixed to the inclusion in which the axes are parallel to those of the global coordinate system x_i ($i = 1, 2, 3$) fixed to the matrix. The x'_i ($i = 1, 2, 3$) is first rotated about the x'_3 -axis through the angle ψ , then about the x'_2 -axis (in its new orientation) through the angle ϕ . In the present case, where an anisotropic

matrix with random distribution of inclusions is considered, special care must be taken on the averaging scheme. We emphasize that the Eshelby tensor is a function of the three Euler angles $\mathbf{S}(\psi, \xi = \cos \theta, \phi)$, the elasticity of the inclusions is just a function of the first two Euler angles $\mathbf{C}_{\text{CNT}}(\psi, \xi = \cos \theta)$ since the transverse isotropy makes these coefficients invariant to ϕ -rotations, and \mathbf{C}_m is fixed. This scheme respects the anisotropy of the matrix and the limits at $f_{\text{CNT}} = 0$ (only matrix) and $f_{\text{CNT}} = 1$ (only the orientational average of the nanoinclusions).

The effective properties of the CNT-modified PVDF matrix are calculated from the anisotropic PVDF elastic coefficients, taken from [11, 26]. These elastic coefficients are listed in table 2.

The effective elastic coefficients obtained by using the approach described above, for the CNT-modified PVDF, are shown in figure 2(e). Notably, both the approaches to model the effective elastic properties of the CNT-modified PVDF matrix lead to similar predictions of effective elastic coefficients, with a linearly increasing trend exhibited by all the coefficients with increase in the carbon nanotube volume fraction.

3. Results and discussion

We divide this section into two subsections. In the first subsection, we discuss the results pertaining to material design and performance with the assumption that PVDF is a mechanically isotropic matrix. In the second subsection, we will compare the predictions of the two material models for PVDF—the well-understood model based on an isotropic elastic assumption and the new model which accounts for the mechanical anisotropy of PVDF.

3.1. Design and performance aspects of CNT-modified PVDF matrices with BaTiO₃ microscale inclusions

We first investigate the effects of adding BaTiO₃ to the PVDF matrix in the absence of MWCNTs. We evaluate the effective piezoelectric coefficients e_{31} and e_{33} using the boundary conditions BC1 and BC2. While these coefficients indicate the sensitivity in terms of generation of electric flux, which is directly useful in the context of strain sensor applications, it is equally important to generate higher electric fields within the composite for energy harvesting material and devices.

In fact, the product of the piezoelectric flux coefficients d and the piezoelectric voltage coefficient g needs to be maximised for optimal energy density in the composites to an applied stress [2, 32], which requires simultaneous maximization of flux and electric fields. Therefore, we compute two other parameters which give an indication of the electric field and the overall performance in the context of energy harvesting—(a) ξ , the volume-averaged electric field component E_3 normalized by the applied strain at the boundary, (b) η_{ij} , the product of the piezoelectric coefficient e_{ij} and ξ which provides an indication of the combined effect of the flux and the electric fields, where the subscripts are in the Voigt's

notation. These are given by:

$$\xi = \frac{|E_3|}{\varepsilon_{\text{app}}}, \eta_{ij} = e_{ij}\xi. \quad (10)$$

3.1.1. The role of BaTiO₃ additions to pristine PVDF matrices. Here we analyze the effect of addition of BaTiO₃ inclusions to a PVDF matrix without CNT-modification. The goal of this analysis is to evaluate the contribution of BaTiO₃ additions on the generation of electric flux and electric fields within the composite. Here we assume the inclusions to be single crystals, i.e. $\alpha = 0$. Figures 3(a)–(c) and (d)–(f) show these effective parameters under the action of two mechanical stimuli given by the boundary conditions BC1 and BC2, respectively. A comparison with a non-piezoelectric matrix with similar elastic properties has been provided, to understand the specific role of the piezoelectricity of PVDF. It is seen that the effective coefficients e_{31} and e_{33} evolve in different ways. The effective coefficient e_{31} of the PVDF-based composite drops with increasing BaTiO₃ additions. This is because of the opposite nature of e_{31} of the matrix and the inclusion due to which addition of BaTiO₃ negates the piezoelectric action of the matrix. In the case of the non-piezoelectric matrix, the e_{31} is negative and increases in magnitude with increasing BaTiO₃ inclusions, as expected. The effective coefficient e_{33} shows a different trend. As more BaTiO₃ is added to the PVDF, the e_{33} becomes increasingly negative (an improvement in the magnitude) initially, although BaTiO₃ has a positive e_{33} . This trend eventually reverses beyond a critical BaTiO₃ loading of roughly $V_{\text{BTO}} = 25\%–30\%$. This is likely due to the large difference in the ε_{11} and ε_{33} permittivity components of BaTiO₃, with the reduced ε_{33} component possibly making lesser contributions to the flux generation governing the effective e_{33} of the composite. In contrast, the non-piezoelectric matrix shows positive e_{33} which increases with addition of BaTiO₃. For very high V_{BTO} , the effective values will approach those of BaTiO₃. However, we restrict our investigation to smaller additions.

Further, the addition of BaTiO₃ inclusions also improves the electric field within the composites. This increase is due to the generated flux exiting from a high permittivity inclusion into a lower permittivity matrix environment. In fact, with even small additions of BaTiO₃, corresponding to $V_{\text{BTO}} = 1.72\%$, there is an enhancement of over 10 orders of magnitude in the volume-averaged absolute electric field. The electric field distribution is further plotted and discussed in the [appendix](#). Therefore, very small additions of such high permittivity piezoelectric materials in PVDF matrices can significantly boost the energy generation capabilities of the composite, with only a small elastic hardening. We are more interested in the product of these quantities as shown in figures 3(c) and (f). It is seen that in the case of boundary condition BC1, η_{31} is significantly higher in the case of the PVDF-based composite than in the case of the non-piezoelectric matrix. This clearly shows that small BaTiO₃ additions to PVDF have definite advantages for energy harvesting, mainly through improved electric fields. The distinct

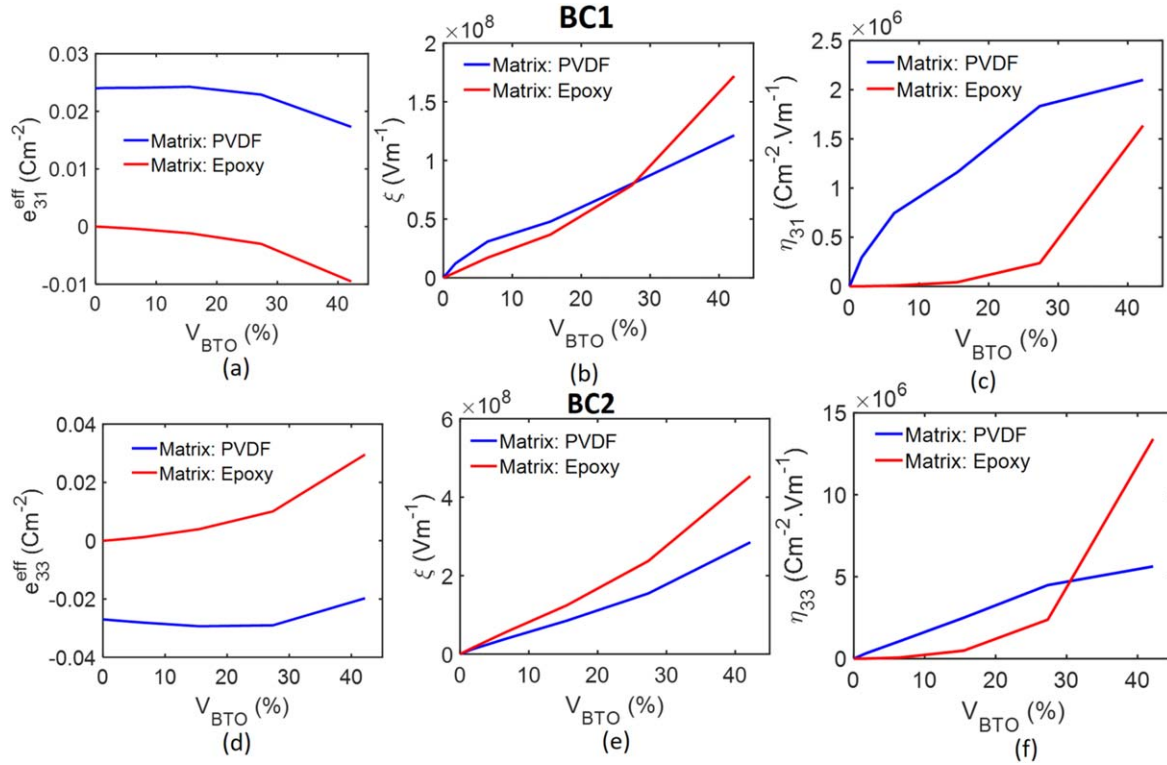


Figure 3. The effective performance parameters obtained from boundary conditions BC1 ((a)–(c)) and BC2 ((d)–(f)). The parameters ξ , η_{31} and η_{33} are defined in equation (3). The data are presented for two matrices—a piezoelectric PVDF and an elastically similar non-piezoelectric epoxy matrix.

advantage of PVDF in such scenarios is its intrinsic piezoelectricity which enables a decent piezoelectric response with small BaTiO₃ additions. This is not seen in the case of the non-piezoelectric matrix where a considerable piezoelectric response occurs only at even higher BaTiO₃ addition. It is evident that at much higher BaTiO₃ concentrations, the non-piezoelectric matrix performs better in terms of its η_{33} . However, this comes at the cost of a very hard composite, and hence we restrict our attention to softer composites with small BaTiO₃ additions and possible applications that this strategy can yield. Both, the effective η_{31} and η_{33} , are better when a PVDF matrix is used with low BaTiO₃ loading, as seen from figures 3(c) and (f). However, as in the case of η_{33} , the non-piezoelectric matrix performs better, due to comparatively better electric flux and electric fields (seen from figures 3(d)–(f)).

3.1.2. The effect of MWCNT-additions to the PVDF matrix on the piezoresponse. We next look at the effect of addition of MWCNTs to the PVDF matrix. We study two composite architectures representing two extreme conditions of BaTiO₃ additions—with a very low V_{BTO} of 1.72% (figures 4(a) and (c)) and a relatively high V_{BTO} of 42.2% (figures 4(b) and (d)), with $\alpha = 0$, corresponding to single crystalline inclusions. In either case, we notice that the role of the MWCNTs is to improve the permittivity of the matrix and consequently couple the flux generated within the inclusions efficiently outwards. However, at low inclusion concentrations, the flux generated by the inclusions is comparable to the flux generated by the matrix and these two components oppose each other, as seen from the

opposite signs of both the piezoelectric parameters of interest (e_{31} and e_{33}) from table 1, in the case of the matrix and the inclusions. Therefore, the effective e_{31} and e_{33} of the composites, under low inclusion concentrations, tend to decrease with an increase in the MWCNT concentration f_{CNT} . However, at much higher BaTiO₃ inclusion concentrations, when the flux generated by the inclusions far exceeds that generated in the matrix, the composite behaviour is predominantly dictated by the nature of the inclusions. Therefore, there is a reversal in the sign of the effective piezoelectric coefficients, as seen from figures 4(b) and (d), and also an order of magnitude improvement in the values compared to the response of the pristine PVDF matrix. We would like to point out that at such high inclusion concentrations, the piezoelectric property of the matrix does not significantly contribute to the response and that similar responses are possible with mechanically similar matrices.

3.1.3. The role of the polycrystallinity of BaTiO₃. We next investigate the role of the polycrystallinity of the BaTiO₃ inclusions. As described earlier, the polycrystallinity is characterized by an orientation parameter α . We simulate the behaviour of the composites, as a function of α , without MWCNTs and with MWCNTs near percolation ($f_{\text{CNT}} = 1.139\%$ where $f_c = 1.14\%$). Further, these simulations are carried out for high inclusion concentrations, particularly $V_{\text{BTO}} = 42.2\%$. The results are shown in figures 5(a), (b) for the piezoelectric PVDF-based and in figures 5(c), (d) for the elastically similar non-piezoelectric epoxy-based composites, respectively. It is seen that in either matrices, the effective

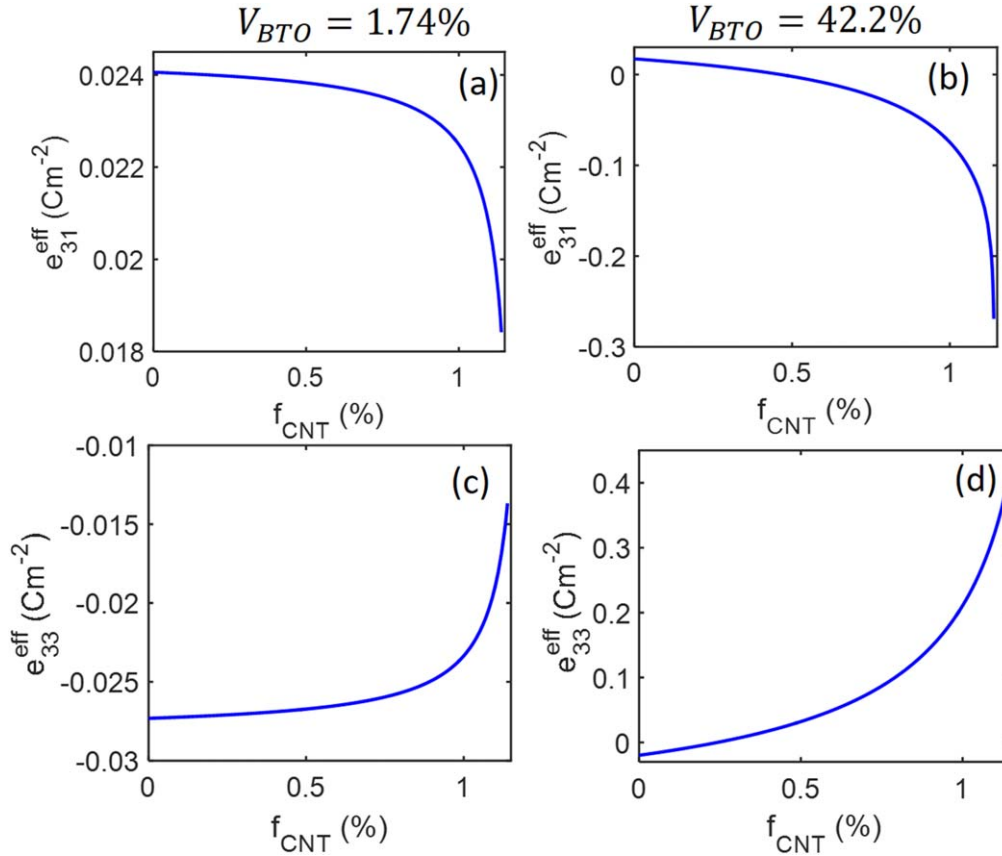


Figure 4. The effective coefficients e_{31} ((a)–(b)) and e_{33} ((c)–(d)) for PVDF/BaTiO₃ composites without CNT additions. The data are presented for two extreme cases of very low BaTiO₃ addition ($V_{BTO} = 1.72\%$ —(a) and (c)) and reasonably high BaTiO₃ addition ($V_{BTO} = 42.2\%$ —(b) and (d)).

coefficients e_{31} and e_{33} are comparable, thus proving that the piezoelectric contribution from the matrix is negligible. The differences in the actual values are mainly due to the slight differences in the elastic properties of the two matrices. Also, it is important to note that an optimal polycrystallinity of $\alpha_{opt} = 0.3$ – 0.4 gives the best piezoelectric response. Although the two matrices differ in their permittivities (3.5 for epoxy and 8 for PVDF) and in their piezoelectric properties, the optimal polycrystallinity is insensitive to these properties. It is important to note here that this optimal value of the polycrystallinity is sensitive to the elastic properties of the matrix, and generally tends to increase as the matrix becomes harder. In particular, we draw attention to our work on elastomeric matrices [16], which have at least an order of magnitude smaller elastic coefficients compared to the epoxy and the PVDF matrices considered here. When such softer matrices are used, we observed an optimal polycrystallinity of $\alpha_{opt} = 0.1$, resulting in maximal piezoelectric response. In summary, we emphasize that the piezoelectric response of PVDF-based lead-free piezocomposites can be improved by addition of MWCNTs. Given the relative softness of PVDF in the x_3 direction, a non-piezoelectric matrix such as the epoxy studied here, might be a better candidate for sensing the ε_{33} strain component. For sensing the ε_{31} strain, when modified by MWCNTs, both the piezoelectric PVDF and the non-piezoelectric epoxy matrices demonstrate similar responses. Further, the optimum polycrystallinity of the BaTiO₃ inclusions

is sensitive to the elastic properties of the matrix, and not to the dielectric and the piezoelectric properties.

3.1.4. The role of BaTiO₃ inclusion concentrations at CNT-percolation. Next, we turn our attention to the effect of the BaTiO₃ inclusion concentration, when the matrices are modified with MWCNTs, under percolative conditions. Under such conditions, the permittivity of the matrix is high and thus there is an efficient decoupling of flux from the inclusions. The nanotubes form a connected network mechanically and electrically, thus simultaneously improving mechanical and electrical coupling within the composite. It is expected that this study will facilitate a comparison with experimentally observed trends [12]. We see from figures 6(a) and (d), that both the effective piezoelectric coefficients, e_{31} and e_{33} , of the composite, show a monotonic behaviour with respect to the inclusion concentration V_{BTO} . This is in good agreement with the experimental observations made on PVDF/BaTiO₃/MWCNT composites [12], indicating that the experimental samples could have percolated nanotube networks. Further, there is also a large improvement in the electric field generated within the composites (figures 6(b) and (e)) and the overall performance parameter η_{ij} (figures 6(c) and (f)). Therefore, addition of MWCNTs to the PVDF matrix provides an overall improvement to the performance of the composite. However,

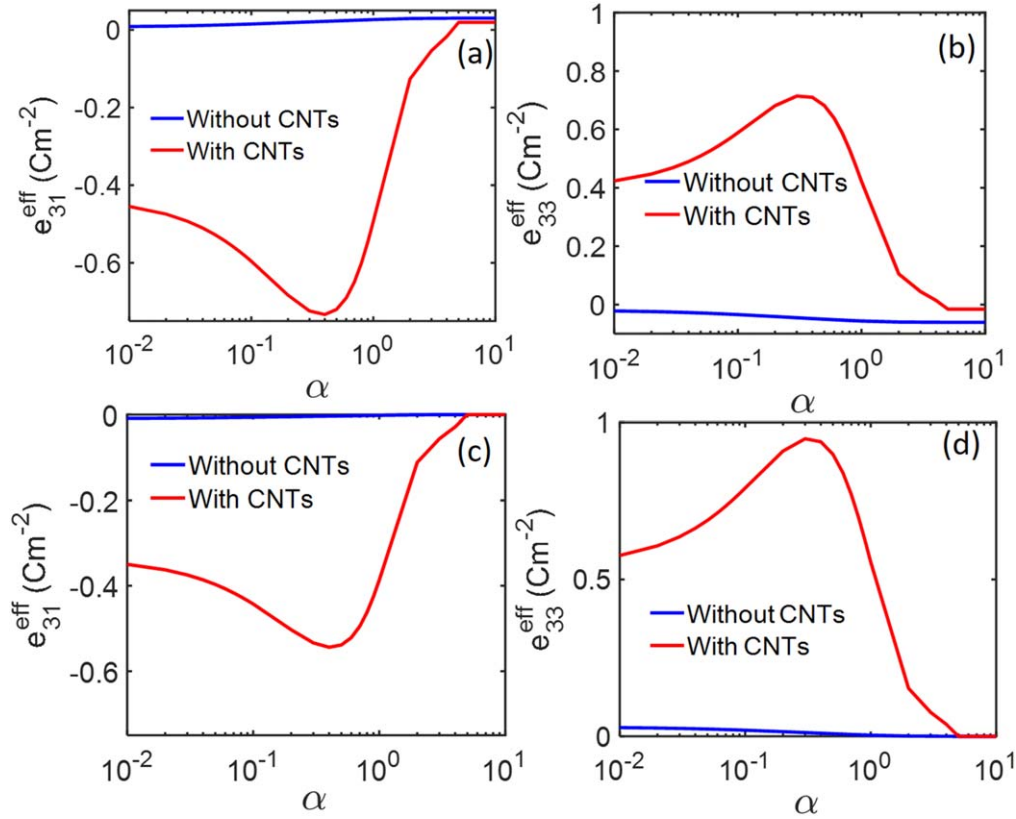


Figure 5. The effective coefficients e_{31} and e_{33} for piezoelectric composites with $V_{\text{BTO}} = 42.2\%$, with a piezoelectric PVDF matrix ((a), (b)) and a non-piezoelectric elastically similar epoxy matrix ((c), (d)). These results are computed with $f_{\text{CNT}} = 0.99f_p$.

since these matrices have percolating nanotube networks, similar performances can be obtained with mechanically similar matrices which are non-piezoelectric [14]. The piezoelectricity of PVDF does not significantly contribute to the response under such conditions.

3.1.5. The combined effects of inclusions and CNT concentrations on overall composite performance. We will finally look at the combined effect of volume fractions of the inclusions and the nanotubes. Of specific interest to us is energy harvesting. We emphasized earlier that the intrinsic piezoelectricity of the matrix is of particular use in the context of energy harvesting from in-plane mechanical stimuli, in flexible electronics. We saw from figure 3(c) that in the absence of nanotubes, a relatively small addition of BaTiO_3 inclusions could lead to significant improvements in the parameter η_{31} corresponding to efficient energy harvesting from in-plane mechanical stimuli. We now will examine the role of the addition of MWCNTs to the matrix on the evolution of the parameter η_{31} . The results are shown in figure 6(g). Firstly, the addition of nanotubes increases the effective η_{31} which indicates possibilities of better energy harvesting. However, the optimal amount of CNT addition is not at percolation, but just below the percolation limit. At percolation, the electric fields generated within the composite drastically drop down and limit the energy harvesting capacity of the composite. Finally, although CNTs lead to improved energy harvesting possibilities, this comes at the cost of an order of magnitude increase in the hardness of the composite. For

example, the effective c_{11} of the composite, shown in figure 6(h) is seen to increase by an order of magnitude near nanotube percolation. This could be useful in the context of rigid energy harvesters. However, specific applications such as flexible energy harvesters might require softer elastic moduli. Figure 6(i) shows the ratio of the η_{31} and the effective elastic coefficient c_{11} of the composite, with two regions of interest: regions A and B. This parameter could be viewed as a metric which exhibits higher values for soft matrices with higher energy harvesting capacities. In region A, the increased CNT concentration increases both the η_{31} and the c_{11} of the matrix, but the increase in η_{31} outweighs the increase in c_{11} , thus resulting in higher values. Note that in region in B, this ratio is still much better compared to the pristine PVDF matrix, although not as high as the composites with nearly percolated nanotube networks. This indicates that there is an ample scope to obtain better performing energy harvesting composites using PVDF, BaTiO_3 inclusions, and a small nanotube addition, as opposed to using a percolated network of nanotubes, which is a typical practice seen in the literature [12]. In the context of sensor applications, however, one needs to consider a more conventional parameter of performance, specifically the effective e_{ij} , which can be obtained using a nearly percolated network of CNTs in the polymer matrix. However, it is not necessary that the matrix be piezoelectric and depending on the details of the application, a non-piezoelectric matrix might be a better candidate for sensor applications. The addition of BaTiO_3 and similar high-permittivity and high-piezoelectric inclusions to a weak-dielectric piezoelectric matrix

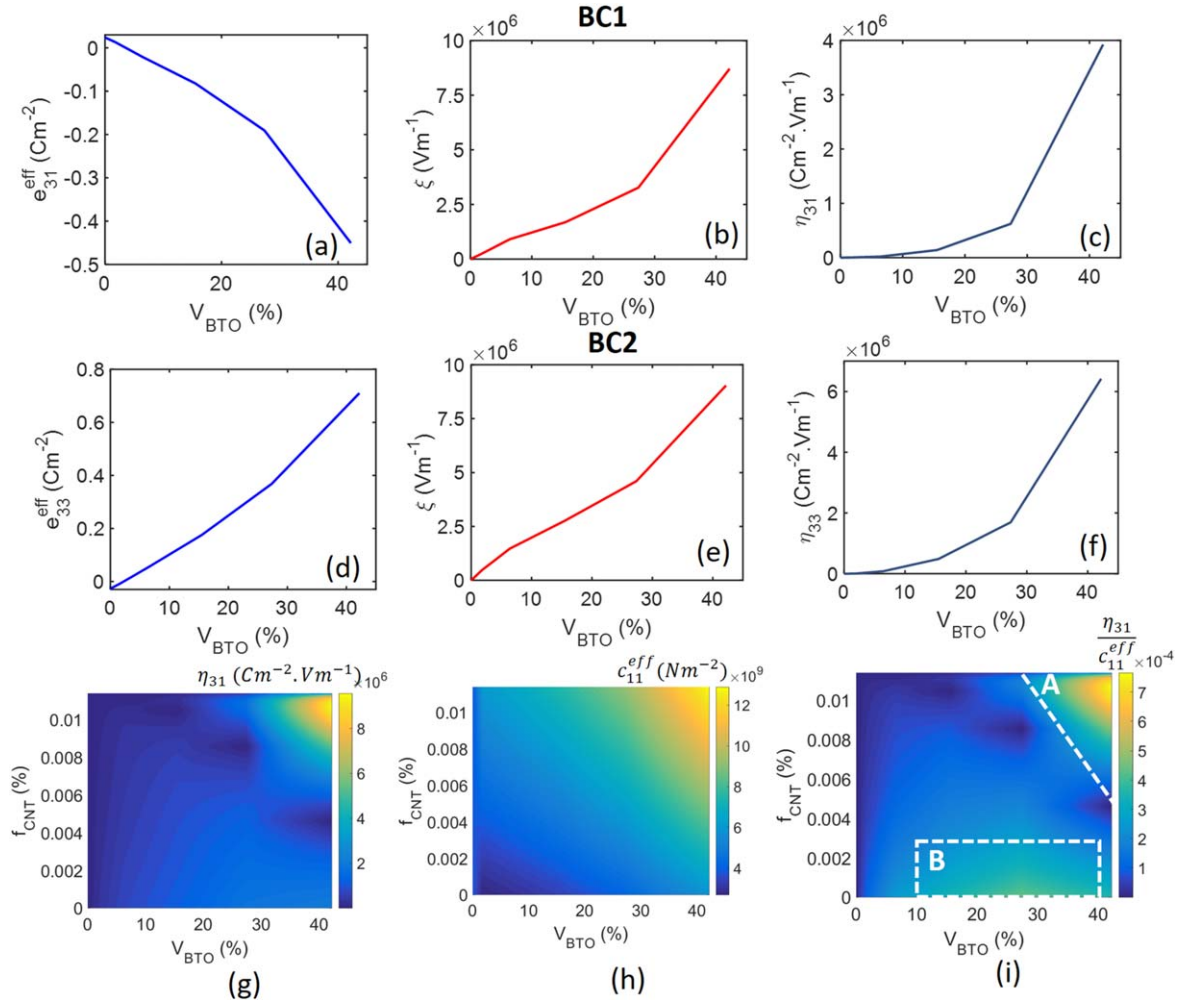


Figure 6. The effective performance parameters e_{ij} , ξ , and η_{ij} obtained from boundary conditions BC1 ((a)–(c)) and BC2 ((d)–(f)). (g)–(i) are plots of η_{31} , c_{11}^{eff} , and $\eta_{31}/c_{11}^{\text{eff}}$ of the composite, as a function of the volume fractions f_{CNT} and V_{BTO} of the CNTs and the BaTiO₃ inclusions, respectively, obtained using boundary condition BC1. Regions A and B in (i) are regions which show considerable improvements in the overall piezoelectric performance for a given matrix hardness.

has significant advantages for energy harvesting, which is not straightforward to obtain using non-piezoelectric matrices.

3.2. Comparison of predictions: the isotropic PVDF assumption versus the anisotropic material model

In this section, we compare the simulations carried out with two effective property models for the PVDF matrix—that derived with an isotropic assumption on the elastic coefficients and that derived accounting for the anisotropy in poled PVDF. Firstly, on comparing the effective elastic properties derived using the isotropic and the anisotropic assumptions, we noticed, that both models predict similar variations in the effective elastic properties i.e. a linearly increasing dependence of the effective elastic coefficients with the CNT concentration f_{CNT} . This shows that the newly developed methodology for calculating the effective properties of an anisotropic material with nano-additions is promising in comparison with the known methods which model isotropic matrices. We further look at the quantity η_{31} , as simulated by both these approaches, shown in figures 7(a) and (b) for the isotropic and the anisotropic assumptions on the PVDF elasticity. The parameter η_{31} is plotted as a function of

f_{CNT} and V_{BTO} . This parameter, as discussed in the earlier sections, depends on both the piezoelectric flux generated and the electric field distribution within the composite. It is seen that both the material models for the effective elastic properties make similar predictions on the effective piezoelectric response. In particular, the variations occurring in η_{31} in terms of the local extrema are present and comparable in both models. The difference in the positions of these extrema could be due to the different mechanical properties used for PVDF, which are taken from different experimental conditions. However, the trends of the parameter η_{31} as a function of CNT and BaTiO₃ loading are predicted equally well by both the models. In fact, the maximum η_{31} (for $V_{\text{BTO}} = 42.2\%$) occurs around $f_{\text{CNT}} = 1.06\%$ in both the predictions, thus further suggesting that the anisotropy in the PVDF matrix may not significantly affect the electromechanical behaviour of the composite. There are, however, differences in the positions of the local minima across the predictions of the two modeling approaches. It is seen that these minima experience a shift towards higher CNT concentrations when the anisotropic model is employed. Also, particularly near CNT percolation, the values of η_{31} are higher as per the anisotropic

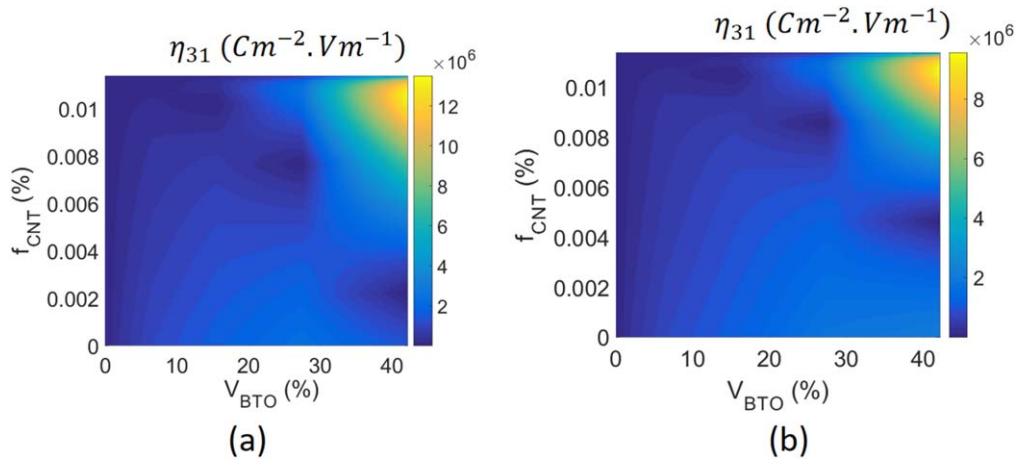


Figure 7. The parameter η_{31} determined by application of boundary condition BC1, for the two different material models assumed for the elasticity of the matrix: (a) an isotropic approximation, and (b) actual anisotropic models.

model. However, since the elastic coefficients for the isotropic and the anisotropic cases are obtained from different experiments, we feel that a detailed conclusion cannot be reached regarding the position of these extrema, at this point. We can, however, say that the overall trends predicted by both the modeling approaches are in good agreement and thus that the elastic anisotropy in PVDF does not significantly affect these trends. Further, the mathematical model developed here for the effective elastic properties of CNT-modified anisotropic media can serve as a key step towards accurate modeling of electro-mechanical responses of composites based on anisotropic matrices.

4. Conclusions

This paper makes contributions towards both design of superior lead-free PVDF-based piezocomposite materials and towards the development of better mathematical models to predict their behaviour accurately. Firstly, based on the assumption that PVDF is elastically isotropic, we have obtained a deeper insight into the criteria underlying improved performance of CNT-modified PVDF based lead-free piezocomposites. Specifically, we note that even a small addition of high-permittivity piezoelectric BaTiO₃ inclusions to a pristine PVDF matrix leads to drastic improvements in the electric fields generated within the composite and consequently significantly improved energy harvesting capabilities. On addition of CNTs to the PVDF matrix, it is seen that at percolative conditions, the piezoelectric coefficients and electric fields generated within the composites are improved significantly with respect to the composite without CNTs. However, it is also important to note that the piezoelectric behaviour of the matrix has negligible contribution to this improved performance. Therefore, for sensing applications, where a high piezoelectric flux generation is required, the piezoelectric properties of the PVDF matrix contribute negligibly and a better sensitivity can be possible through the use of non-piezoelectric matrices modified by CNTs. At the same time, in the area of energy harvesting, we note that small additions of BaTiO₃ and CNTs, away from the percolation conditions which

are traditionally employed, can lead to dramatic improvements in the energy harvesting capabilities of the composite, through orders of magnitude improvement in the electric field generation within the composite. Notably, we see that it is possible to effect significant improvement in energy harvesting capabilities of the composite through even small additions of BaTiO₃ and CNTs, without considerable hardening of the composite. Further, we have developed a new mathematical paradigm for calculating the effective elastic properties of the CNT-modified elastically anisotropic matrices such as PVDF. The predictions made using the new model bears excellent agreement with the trends predicted by the well understood model based on isotropic elasticity assumed in the PVDF. This suggests that the anisotropy in PVDF might not be a significant factor in fixing the piezoelectric response of the composite. In summary, the paper offers deeper insights into the design of efficient PVDF-based lead-free piezocomposites for sensing and energy harvesting and in addition, develops new mathematical models for describing composites with elastically anisotropic nano-modified matrices.

Acknowledgments

This work was supported by the Ministerio de Economía y Competitividad of Spain and the European Regional Development Fund under projects RTI2018-094945-B-C21 and DPI2017-89162-R. The financial support is gratefully acknowledged. RM and AKJ are also grateful to the NSERC and CRC program for their support.

Appendix. Enhanced electric fields on BaTiO₃ addition to PVDF

As discussed in the main part of the paper, one of the key advantages of adding BaTiO₃ (or other piezoelectric crystalline inclusions exhibiting high permittivity and high piezo-response) is probably the dramatic increase in the electric field generation within the composite. These fields are generated when the piezoelectric flux flows from the high permittivity

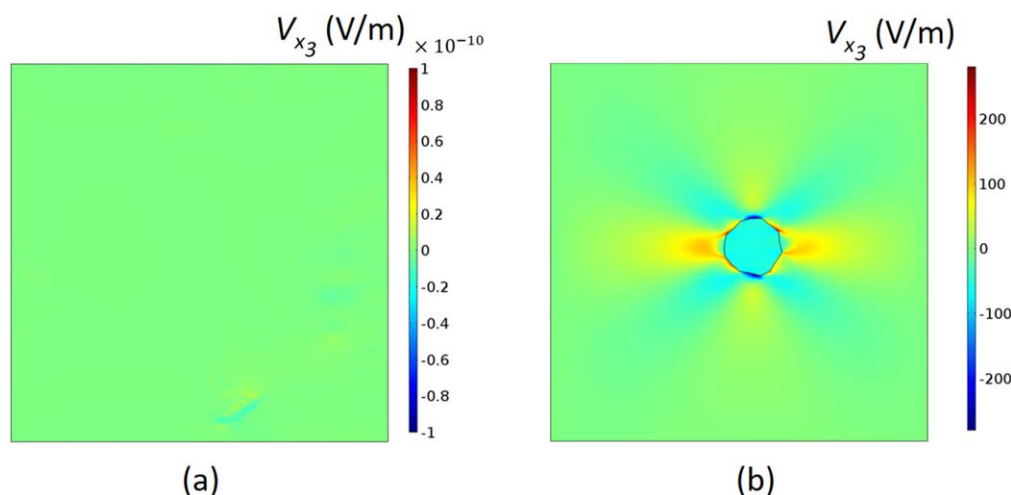


Figure A1. The electric field (x_3 component) distribution in (a) pristine PVDF and (b) PVDF + 1.72%(vol) BaTiO₃ when subjected to boundary condition BC1, with $\epsilon_a = 1 \times 10^{-6}$.

inclusion to the low permittivity matrix. Even very small additions of BaTiO₃, of around 1.72%, can lead to a significant boost of 10–11 orders of magnitude in the volume-averaged absolute electric field, as seen in the distribution of the x_3 component of the electric field in figure A1 for the pristine PVDF and the composite with 1.72% vol BaTiO₃.

ORCID iDs

Jagdish A Krishnaswamy <https://orcid.org/0000-0001-7451-3237>

Enrique García-Macías <https://orcid.org/0000-0001-5557-144X>

Luis Rodriguez-Tembleque <https://orcid.org/0000-0003-2993-8361>

References

- [1] Ibn-Mohammed T, Koh S, Reaney I, Sinclair D, Mustapha K, Acquaye A and Wang D 2017 Are lead-free piezoelectrics more environmentally friendly? *MRS Commun.* **7** 1–7
- [2] Maurya D, Peddigari M, Kang M-G, Geng L D, Sharpes N, Annappureddy V, Palneedi H, Sriramdas R, Yan Y and Song H-C 2018 Lead-free piezoelectric materials and composites for high power density energy harvesting *J. Mater. Res.* **33** 2235–63
- [3] Tiller B, Reid A, Zhu B, Guerreiro J, Domingo-Roca R, Curt Jackson J and Windmill J F C 2019 Piezoelectric microphone via a digital light processing 3D printing process *Mater. Des.* **165** 107593
- [4] Kim H, Torres F, Villagran D, Stewart C, Lin Y and Tseng T L B 2017 3D printing of BaTiO₃/PVDF composites with electric *in situ* poling for pressure sensor applications *Macromol. Mater. Eng.* **302** 1700229
- [5] Kim K, Zhu W, Qu X, Aaronson C, McCall W R, Chen S and Sirbulu D J 2014 3D optical printing of piezoelectric nanoparticle-polymer composite materials *ACS Nano* **8** 9799–806
- [6] Lee M, Chen C Y, Wang S, Cha S N, Park Y J, Kim J M, Chou L J and Wang Z L 2012 A hybrid piezoelectric structure for wearable nanogenerators *Adv. Mater.* **24** 1759–64
- [7] Phatharapeetranun N, Ksapabutr B, Marani D, Bowen J R and Esposito V 2017 3D-printed barium titanate/poly-(vinylidene fluoride) nano-hybrids with anisotropic dielectric properties *J. Mater. Chem. C* **5** 12430–40
- [8] Ghosh S K, Adhikary P, Jana S, Biswas A, Sencadas V, Gupta S D, Tudu B and Mandal D 2017 Electrospun gelatin nanofiber based self-powered bio-e-skin for health care monitoring *Nano Energy* **36** 166–75
- [9] Seminara L, Capurro M, Cirillo P, Cannata G and Valle M 2011 Electromechanical characterization of piezoelectric PVDF polymer films for tactile sensors in robotics applications *Sensors Actuators A* **169** 49–58
- [10] Cui H, Hensleigh R, Yao D, Maurya D, Kumar P, Kang M G, Priya S and Zheng X R 2019 Three-dimensional printing of piezoelectric materials with designed anisotropy and directional response *Nat. Mater.* **18** 234
- [11] Odegard G M 2004 Constitutive modeling of piezoelectric polymer composites *Acta Mater.* **52** 5315–30
- [12] Kim H, Torres F, Islam M T, Islam M D, Chavez L A, Rosales C A G, Wilburn B R, Stewart C M, Noveron J C and Tseng T-L B 2017 Increased piezoelectric response in functional nanocomposites through multiwall carbon nanotube interface and fused-deposition modeling three-dimensional printing *MRS Commun.* **7** 960–6
- [13] Kim H, Torres F, Wu Y, Villagran D, Lin Y and Tseng T-L B 2017 Integrated 3D printing and corona poling process of PVDF piezoelectric films for pressure sensor application *Smart Mater. Struct.* **26** 085027
- [14] Kim H J and Kim Y J 2018 High performance flexible piezoelectric pressure sensor based on CNTs-doped 0–3 ceramic-epoxy nanocomposites *Mater. Des.* **151** 133–40
- [15] Qi F, Chen N and Wang Q 2018 Dielectric and piezoelectric properties in selective laser sintered polyamide11/BaTiO₃/CNT ternary nanocomposites *Mater. Des.* **143** 72–80
- [16] Krishnaswamy J A, Buroni F C, Garcia-Sanchez F, Melnik R V, Rodriguez-Tembleque L and Saez A 2019 Improving the performance of lead-free piezoelectric composites by using polycrystalline inclusions and tuning the dielectric matrix environment *Smart Mater. Struct.* **28** 075032
- [17] Saputra A A, Sladek V, Sladek J and Song C 2018 Micromechanics determination of effective material coefficients of cement-based piezoelectric ceramic composites *J. Intell. Mater. Syst. Struct.* **29** 845–62

- [18] Lee J S, Kim G H, Kim W N, Oh K H, Kim H T, Hwang S S and Hong S M 2008 Crystal structure and ferroelectric properties of poly (vinylidene fluoride)-carbon nano tube nanocomposite film *Mol. Cryst. Liq. Cryst.* **491** 247–54
- [19] Zheng P, Zhang J, Tan Y and Wang C 2012 Grain-size effects on dielectric and piezoelectric properties of poled BaTiO₃ ceramics *Acta Mater.* **60** 5022–30
- [20] Kim G H, Hong S M and Seo Y 2009 Piezoelectric properties of poly (vinylidene fluoride) and carbon nanotube blends: β -phase development *Phys. Chem. Chem. Phys.* **11** 10506–12
- [21] Yao S-H, Dang Z-M, Jiang M-J, Xu H-P and Bai J 2007 Influence of aspect ratio of carbon nanotube on percolation threshold in ferroelectric polymer nanocomposite *Appl. Phys. Lett.* **91** 212901
- [22] Wang L and Dang Z-M 2005 Carbon nanotube composites with high dielectric constant at low percolation threshold *Appl. Phys. Lett.* **87** 042903
- [23] Pecharroman C, Esteban-Betegon F, Bartolome J F, Lopez-Esteban S and Moya J S 2001 New percolative BaTiO₃-Ni composites with a high and frequency-independent dielectric constant ($\epsilon_r \approx 80000$) *Adv. Mater.* **13** 1541–4
- [24] Li J Y 2000 The effective electroelastic moduli of textured piezoelectric polycrystalline aggregates *J. Mech. Phys. Solids* **48** 529–52
- [25] Rodríguez-Tembleque L, García-Macías E and Sáez A 2018 CNT-polymer nanocomposites under frictional contact conditions *Composites B* **154** 114–27
- [26] Shen L and Li J 2005 Transversely isotropic elastic properties of multiwalled carbon nanotubes *Phys. Rev. B* **71** 035412
- [27] Shi D-L, Feng X-Q, Huang Y Y, Hwang K-C and Gao H 2004 The effect of nanotube waviness and agglomeration on the elastic property of carbon nanotube-reinforced composites *J. Eng. Mater. Technol.* **126** 250–7
- [28] Vinogradov A and Holloway F 1999 Electro-mechanical properties of the piezoelectric polymer PVDF *Ferroelectrics* **226** 169–81
- [29] Pu J, Yan X, Jiang Y, Chang C and Lin L 2010 Piezoelectric actuation of direct-write electrospun fibers *Sensors Actuators A* **164** 131–6
- [30] Raponi O d A, Raponi R d A, Barban G B, Benedetto R M D and Ancelotti Junior A C 2017 Development of a simple dielectric analysis module for online cure monitoring of a commercial epoxy resin formulation *Mater. Res.* **20** 291–7
- [31] Mura T 2013 *Micromechanics of Defects in Solids* (Berlin: Springer)
- [32] Priya S 2010 Criterion for material selection in design of bulk piezoelectric energy harvesters *IEEE Trans. Ultrason. Ferroelectr. Freq. Control* **57** 2610–2